Convective cell dynamics in universal drift wave turbulence

斉藤, 剛
九州大学大学院総合理工学府

伊藤, 早苗
九州大学応用力学研究所

矢木, 雅敏
九州大学応用力学研究所

https://doi.org/10.15017/3549

出版情報：九州大学応用力学研究所所報. 127, pp.13-25, 2004-09. Research Institute for Applied Mechanics, Kyushu University
バージョン：
権利関係：

Convective cell dynamics in universal drift wave turbulence

Tsuyoshi SAITO *1, Sanae-I. ITOH *2, Masatoshi YAGI*2,

E-mail of corresponding author: *tsuyoshi@riam.kyushu-u.ac.jp*

(Received July 30, 2004)

Abstract

The interaction between the universal drift wave and the convective cell in the shearless slab geometry is investigated using a kinetic-fluid model based on nonlinear gyro-kinetic equations. It is found that the convective cell is nonlinearly excited in a way, which is similar to the zonal flow generation of ITG turbulence. On the other hand, if we introduce the large ion-ion collision effect, the zonal flow is damped and instead the streamer and finite ky modes are excited in the convective cell mode. As the result, the flux is larger than the one without collision. The forward cascade is observed in kz space and the forward/inverse cascade is observed in ky space in the time evolution of energy spectrum.

Key words : *Universal drift wave, Convective cell, Zonal flow, Streamer, Nonlinear simulation, The effect of ion-ion collision, Kinetic-fluid model*

1. Introduction

Research on anomalous transport in high temperature plasmas is important issue in thermo-nuclear fusion research. It is considered that the drift wave contributes to anomalous transport. The ion temperature gradient (ITG) driven turbulence is caused by the drift wave destabilized by the ion temperature gradient. Recently, there has been a considerable progress in the gyro-kinetic particle-in-cell simulation of ITG driven turbulence [1, 2]. These simulations have demonstrated that zonal flows [3] play a crucial role in regulating drift wave turbulence and the level of the anomalous ion transport. The theoretical explanation for the generation of zonal flow has been proposed based on a modulational instability [4, 5]. Later, a four-mode model of zonal flow growth in toroidal geometry has been developed [6]. While works [4, 5, 6] have provided a firm theoretical foundation on this subject, the direct comparisons to the gyro-kinetic simulation results have been only possible in certain idealized cases. Simplified assumptions made for analytic theory are not always satisfied in simulations of turbulence. It is worth performing the simulations in a simplified geometry and comparing the results with those from the theory.

In this thesis, a kinetic-fluid model [7] in a shearless slab geometry is used to study the problem. This model is an extension of the model proposed by Smolyakov [8] and Hinton [9], which include the nonlinear interaction between z-axisymmetric potentials in zonal flows and z-nonaxisymmetric potentials in drift waves [9]. The adiabatic electron is assumed, therefore, no unstable drift wave is included. They assume the marginally stable drift wave with $\omega_i = 0$. Our model can describe the universal drift wave turbulence and nonlinear excitation of convective cells (CC) [11], in which zonal flows and streamers by drift waves are included. The schematic diagram of zonal flow and streamer is described in Fig.1. The zonal flow and the streamer are one of Fourier components which constitute the convective cell. In chapter 2, we review simulation and theory of drift wave turbulence and convective cell dynamics in later 70's, and the recent theory of ITG and zonal flow turbulence dynamics. In chapter 3, we explain our model equations. In chpater 4, simulation results are discussed. Finally, discussion and summary are given in chapter 5.

2. Review

2.1 Convective Cell

2.1.1 Numerical Simulation of Drift Wave Turbulence

In later 70's, three dimensional particles simulations were performed on the collisionless drift instabilities in a cylindrical geometry [11]. The simulation

*1 Interdisciplinary Graduate School of Engineering Sciences, Kyushu University
*2 Research Institute for Applied Mechanics, Kyushu University

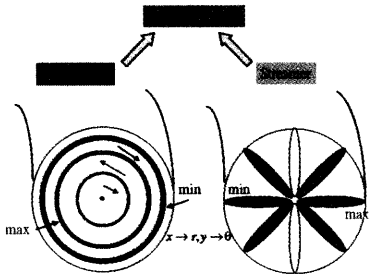

Fig. 1 Schematic diagram of zonal flow and streamer. Red lines expresses maximum amplitude, blue lines expresses minimum amplitude of the wave

model used was a straight cylinder in an uniform external magnetic field B_0 in the z direction with its length $L_z/\rho_i = 640$, $\rho_i = (T_i/m_i)^{1/2}/\Omega_i$ being the ion gyroradius, where m_i is the ion mass, T_i is the ion temperature and Ω_i is the ion cyclotron frequency. For numerical computation with its physical length $L/\rho_i = 32$, a 64×64 (L^2) spatial grid was used. The plasma was assumed to be periodic in z direction. Initial conditions of ions and electrons had Maxwellian velocity distributions with $T_e/T_i = 4$, where T_e is the electron temperature. Initial plasma density profile was taken to be $n_e(r) = n_i(r) = n_0 exp(-4r^2/a^2)$ with the average density given by $\Omega_e/\omega_{Pe} = 5, m_i/m_e = 100, a = L/2$, where Ω_e is the electron cyclotron frequency, ω_{Pe} is the electron plasma frequency and a is a half width of density profile; and there was no initial temperature gradient. Seven Fourier modes $n = 0, \pm1, \pm2, \pm3$, where n is the Fourier mode number in z direction and the mode with $n = 0(\omega = 0)$ is defined as convective-cell mode, were kept in z direction with the wave number $k_z = 2\pi n/L_z$. Linear analysis predicts that the collisionless drift instability (universal mode) is strongly unstable against $n = \pm1$ perturbations, which becomes stable with increasing $|n|$ due to the onset of ion Landau damping.

Fig.2 shows the particle diffusion, heat transfer, electron velocity distribution, and radial-mode structure for the $\frac{e\phi_{mn}}{T_e}$ associated with the instability of the electrostatic potential ϕ_{mn}, where m is the azimuthal mode number with $k_\theta = m/r$. While ions and electrons diffuse more or less together in the early stage, large charge separation built up at a later stage. This is because of the difference of radial cE_θ/B drifts of ions and electrons, where E_θ is the fluctuating azimuthal electric field associated with the drift wave. The observed anomalous particle diffusion was mainly due to drift instabilities at the early stage. At the later stage, it was due to nonlinearly excited convective cells, which enhance the diffusion even when the drift instability is quenched.

The electron parallel temperature $T_{e\|}$ rapidly decreases for $r/a > 0.5$ because of the inverse Landau damping. It increases for $r/a < 0.5$ because of the absorption of wave energy. The electron parallel velocity distribution is steepened because of inverse Landau damping. Ion perpendicular temperature $T_{i\perp}$ increases due to the convective cells. Ion parallel temperature $T_{i\|}$ changes little because the contribution from the ion Landau damping is weak. A typical drift-wave radial mode-structure of $|e\phi_{mn}(r)/T_e|$ with $m/n = 3/1$ shows a peak near $r/a = 0.5$ at the early stage. After reaching the maximum amplitude of 10% at $\omega_{Pe}t = 1040$, it begins to decrease as a result of nonlinear excitation of convective cells ($n = 0, \omega = 0$).

Fig.3 shows more detailed diagnostic of the instability: spectral distributions $|E^2(m)|$ and $|E^2(n)|$, and power spectrum $P_{mn}(\omega, r)$ where $|E^2(m)| = \sum_n |\frac{e\phi_{m,n}(t,r)}{T_e}|^2$, $|E^2(n)| = \sum_m |\frac{e\phi_{m,n}(t,r)}{T_e}|^2$ and $P_{mn}(\omega, r) = |\frac{e\phi_{m,n}(\omega,r)}{T_e}|^2$. $|E^2(m)|$ indicates typical spectral profile for drift turbulence as seen in the experiments; it peaks around $k_\theta\rho_i = 0.3 \sim 0.6$, corresponding to the $m = 2, 3$ and 4 modes for this case. The amplitude decreases rapidly for $k_\theta\rho_i \geq 1$ ($m \geq 8$). The shape of the spectral distribution little changes from early stage. The shift of the peak of the spectrum toward low m numbers was seen. The shift of peak was due to the nonlinear excitation of convective cells which tend to coalesce into large cells. $|E^2(n)|$, on the other hand, shows a drastic change when the instability develops into a nonlinear regime. We see that at earlier times the spectrum was peaked at $n = 1$ ($k_z = 2\pi/L_z$) and decreases rapidly with increasing n. The $n = 0$ mode, which may be called 'convective-cell mode' ($k_z = 0, \omega = 0$), also grows as the drift instability grows; and eventually they dominate over the drift instability. Note that this state is not the ambipolar field ($m = n = 0$) (it is called zonal flow in the recent terminology). The excitation of convective cells is clearly seen in the power-spectrum plots $P_{mn}(\omega)$ at $r/a = 0.5$, where we see both drift modes ($n \neq 0, \omega \neq 0$) and convective cells ($n = 0, \omega = 0$). For the case of $m = 3$ mode, the power spectrum indicates that the amplitude of drift mode ($n = 1$) was much larger than that of the convective cells ($n = 0$), while for $m = 1$ case , convective cell components are much stronger than the drift mode ones.

2.1.2 Nonlinear Mechanism for Excitation of Convective Cell

In this section, the theoretical work for the excitation of CC is reviewed. It is based on the decay instability.

A system of equations describing the nonlinear interaction of the drift waves with the convective mode are

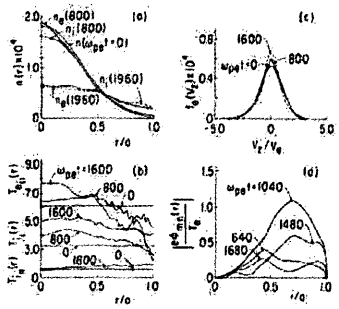

Fig. 2 Time variation of (a) ion and electron density profiles $n_i(r)$ and $n_e(r)$ in terms of number of particles summed over a given volme; (b) electron parallel temperature $T_{e\parallel}(r)$, ion parallel temperature $T_{i\parallel}(r)$, and ion perpendicular temperature $T_{i\perp}(r)$ in terms of thermal electron energy $m_e v_e^2/2 = 6.2$; (c) electron velocity distribution; and (d) radial-mode structures for the $(m,n) = (3,1)$ mode.

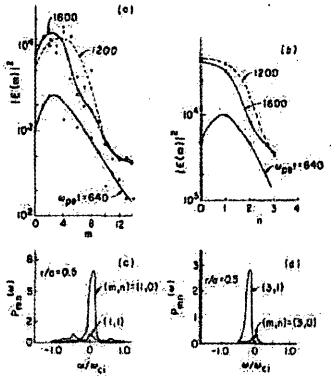

Fig. 3 Time variation of (a) spectral distribution $|E^2(m)|$ and spectral distribution $|E^2(n)|$. Power spectra for (c) the $(m,n) = (1,1)$ and $(1,0)$ modes indicate two peaks near $\omega \approx 0$ and ω^*.

written by [13]

$$\frac{\partial n}{\partial t} + \frac{c}{H}\left(\frac{\partial \phi}{\partial x}\frac{\partial n}{\partial y} - \frac{\partial \phi}{\partial y}\frac{\partial n}{\partial x}\right) - \frac{c}{H}\frac{n_0}{\omega_{Hi}}\left(\frac{\partial}{\partial t} - \mu\Delta\right)\Delta U - \frac{c^2}{H^2}\frac{1}{\omega_{Hi}}\left[\frac{\partial}{\partial x}n_0\left(\frac{\partial \phi}{\partial x}\frac{\partial}{\partial y} - \frac{\partial \phi}{\partial y}\frac{\partial}{\partial x}\right)\cdot\frac{\partial U}{\partial x} + \frac{\partial}{\partial y}n_0\left(\frac{\partial \phi}{\partial x}\frac{\partial}{\partial y} - \frac{\partial \phi}{\partial y}\frac{\partial}{\partial x}\right)\cdot\frac{\partial U}{\partial y}\right] = 0 \qquad (1)$$

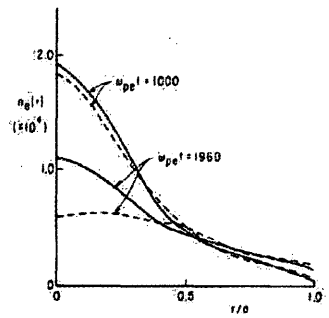

Fig. 4 Comparison of electron density diffusion with and without convective cells $(k_l) = 0$. Note that at $\omega_{Pe}t = 1960$, convective cells have larger amplitudes than the drift waves when the convective cells are not delected.

$$\frac{\partial n}{\partial t} + \frac{c}{H}\left(\frac{\partial \phi}{\partial x}\frac{\partial n}{\partial y} - \frac{\partial \phi}{\partial y}\frac{\partial n}{\partial x}\right) + n_0\frac{\partial v_{ze}}{\partial z} = 0 \qquad (2)$$

Here $\mu = \frac{3}{10}\frac{T_i}{m_i\omega_{Hi}^2}\nu_i$ is the ion viscosity, $U = \phi + (T_i/e)\ln n$ is the generalized potential (ϕ is the electrostatic potential), and $\Delta = \partial^2/\partial x^2 + \partial^2/\partial y^2$. The last term in eq.(2) describes the density perturbation due to the longitudinal electron motion and is important only for the drift mode, where H ($B = \mu H$) is the magnetic intensity and ω_{Hi} is the cyclotron frequency.

All quantities corresponding to the collective particle motions were separated into two parts, describing the drift and convective cell modes, respectively as:

$$\phi = \phi^c(t,x,y) + \phi^d(t,r)$$
$$\delta n = \delta n^c(t,x,y) + \delta n^d(t,r) \qquad (3)$$

where superfix c and d denote the convective cell and drift wave, respectively. For the existence of the drift wave, the condition $|\omega^d| \ll k_z v_{Te}$ holds, so the Boltzman distribution was always established because of the fast electron motion in the longitudinal direction;

$$\phi^d = \frac{T_e}{e}\ln\left[1 + \frac{\delta n^d}{n_0(x) + \delta n^c}\right] \qquad (4)$$

Using eq.(4) and assuming that $\delta n^c \ll n_0$ and $|\frac{1}{k}\frac{d}{dx}\ln n_0| \ll 1$, the equations for the density and the potential variation in the drift wave are obtained from eq.(1). For the slow mode of plasma motions which are homogeneous along the magnetic field, we obtain the following system of equations from eqs.(1) and (2):[13]

$$\frac{\partial \delta n^c}{\partial t} - \frac{c}{H}\frac{\partial \phi^c}{\partial y}\frac{dn_0}{dx} = \frac{c}{H}\left(\frac{\partial \phi^c}{\partial y}\frac{\partial \delta n^c}{\partial x} - \frac{\partial \phi^c}{\partial x}\frac{\partial \delta n^c}{\partial y}\right) \qquad (5)$$

$$\left[\frac{\partial}{\partial t}-\mu\Delta+\frac{c}{H}\left(\frac{\partial\phi^c}{\partial x}\frac{\partial}{\partial y}-\frac{\partial\phi^c}{\partial y}\frac{\partial}{\partial x}\right)\right]\Delta U^c$$
$$+\frac{c}{H}\left[\left(\frac{\partial^2\phi^c}{\partial x^2}-\frac{\partial^2\phi^c}{\partial y^2}\right)\frac{\partial^2 U^c}{\partial x\partial y}-\left(\frac{\partial^2 U^c}{\partial x^2}-\frac{\partial^2 U^c}{\partial y^2}\right)\frac{\partial^2\phi^c}{\partial x\partial y}\right]$$
$$=D_B\frac{T_e}{en_0^2}\left\langle\left(\frac{\partial\delta n^d}{\partial y}\frac{\partial}{\partial x}-\frac{\partial\delta n^d}{\partial x}\frac{\partial}{\partial y}\right)\Delta\delta n^d\right\rangle_z, \qquad (6)$$

where $U^c=\phi^c+(T_i/e)(\delta n^c/n_0)$ and D_B is the Bohm diffusion coefficient. The angle brackets on the right hand side of eq.(6) denote an averaging over a spatial interval $\sim 1/k_z$. The nonlinear terms retained on the left hand side of eq.(6) are responsible for the inherent nonlinearity of the $k_z=0$ mode and describe the energy pumping between different $k_\perp$ scales. The terms in the right hand side of eq.(6) are responsible for the excitation of $k_z=0$ mode in the nonlinear interaction of drift waves.

Assuming that the contribution to anomalous plasma transport is due to slower mode of the convective cells, the analysis is restricted below to this mode, and assumes $|\omega^c|\ll\omega_i^d$, which corresponds to $e\phi^c\ll T_i(\delta n^c/n_0)$. Using the latter condition and omitting those terms which are responsible for the inherent nonlinearity of the drift waves and convective mode, the following system of equations, which describes the interaction of the drift waves and convective cells, is finally derived [13].

$$\frac{\partial\delta n^d}{\partial t}-D_B\frac{d\ln n_0}{dx}\frac{\partial\delta n^d}{\partial y}-\rho_i^2\frac{\partial}{\partial t}\Delta\delta n^d$$
$$=-\frac{D_B}{n_0}\left(\frac{\partial\delta n^d}{\partial x}\frac{\partial\delta n^c}{\partial y}-\frac{\partial\delta n^d}{\partial y}\frac{\partial\delta n^c}{\partial x}\right) \qquad (7)$$

$$\left(\frac{\partial}{\partial t}-\mu\Delta\right)\Delta\delta n^c$$
$$=D_B\frac{T_e}{T_in_0}\left\langle\left(\frac{\partial\delta n^d}{\partial y}\frac{\partial}{\partial x}-\frac{\partial\delta n^d}{\partial x}\frac{\partial}{\partial y}\right)\Delta\delta n^d\right\rangle \qquad (8)$$

The dispersion relation of the drift waves in eq.(7),

$$\omega^d=-k_yD_B\frac{d\ln n_0}{dx}\frac{1}{1+k_\perp^2\rho_i^2} \qquad (9)$$

follows from the general equation for the drift frequency [12]:

$$\omega^d=-k_yD_B\frac{d\ln n_0}{dx}\frac{\Gamma(\xi)}{1+\frac{T_e}{T_i}(1-\Gamma(\xi))} \qquad (10)$$

in the limit of $T_i\ll T_e$, $k_\perp\rho_i(T_i/T_e)^{1/2}\ll 1$, where $\Gamma(\xi)=e^{-\xi}I_0(\xi)$ and $\xi=k_\perp^2\rho_i^2\frac{T_i}{T_e}$.

In the short-wave length part of the spectrum, $k_\perp\rho_i\sim 1$, we can always distinguish the waves with identical values of ω and k_z (and different values of k_x and k_y), which interact and give rise to convective cells (Fig.5). This is described in the right side of eq.(8) since an averaging over the spatial interval $\sim k_z^{-1}$ and over the fast time $(\omega_d)^{-1}$ is taken.

A simplest mechanism for the nonlinear generation of convective motions is known to be the decay instability of a monochromatic drift wave. Let us examine the decay instability of a mode which is localized along the x direction

$$\delta n^d=\delta n_0(x)\exp(ik_{y0}y+ik_{z0}z-i\omega_0^dt)$$
$$+\delta n_1(x)\exp(ik_{y1}y+ik_{z0}z-i\omega_0^dt-i\omega t)+c.c. \qquad (11)$$

$$\delta n^c=\delta n_2(x)\exp(ik_{y2}y-i\omega t)+c.c. \qquad (12)$$

where the subscript "0" refers to the fundamental wave, "1" refers to the test drift wave, and $\mathbf{k_2}=\mathbf{k_1}-\mathbf{k_0}$. Substituting this equation into eqs.(7) and (8) the equation for δn_2 is obtained as

$$\frac{d^2\delta n_2}{dx^2}+\left[\frac{\omega(\omega+i\mu k_{y2}^2)}{D_B^2}\frac{T_i}{T_e}\frac{n_0^2}{(\delta n_0)^2}\frac{k_{y2}^2}{k_{y0}^2(k_{y1}^2-k_{y0}^2)}\right.$$
$$\left.+\frac{k_{y0}^2-k_{y1}^2}{k_{y0}^2}\frac{1}{(\delta n_0)^2}\left(\frac{d\delta n_0}{dx}\right)^2-\frac{k_{y1}}{k_{y0}}\frac{d^2}{dx^2}\ln\delta n_0\right]\delta n_2$$
$$=0 \qquad (13)$$

Multiplying eq.(13) by δn_2 and integrating it over the plasma slab, $-a\le x\le a$ and assuming that the spatial region to which the convective mode is confined is much smaller than the drift wave region, $\Delta^c\ll\Delta^d$, we obtain the following approximate equation for the instability growth rate

$$\gamma^d=D_Bk_{y0}k_x^c\sqrt{\frac{T_e}{T_i}\left(\frac{\delta n_0}{n_0}\right)^2\frac{k_{y0}^2-k_{y1}^2}{k_{y2}^2}} \qquad (14)$$

where $k_x^c=\pi/\Delta^c$. It is found that the characteristic time of the convective mode growth in numerical simulations agrees with that for the decay instability of drift waves.

The mechanism for the nonlinear generation of convective cells studied here is extremely important to magnetic plasma confiment, since it is obvious that the slow plasma motions in these cells can substantially raise the diffusion confinement, as demonstrated in the numerical simulations [11].

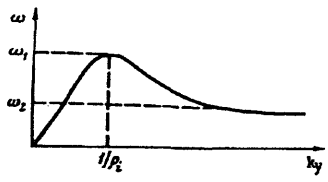

Fig. 5 Dispersion of drift waves in a non-isothermal ($T_e>T_i$) plasma. $\omega_1=-D_B\frac{d\ln n_0}{dx}/2\rho_i$, $\omega_2=\sqrt{\frac{2}{\pi}\frac{T_i}{T_e}}\omega_1$

2.2 Dynamics of Zonal Flows and Drift Wave Turbulence

In this section, the recent theoretical works on the zonal flow generation in ITG turbulence is reviewed. Zonal flows [13] are poloidally and toroidally symmetric ($k_\theta = k_z = 0$), zero-frequency ($\omega = 0$) vortex modes with finite radial scale (k_r finite), and thus constitute a limiting case of the more general notion of a "convective cell" [14]. Since zonal flows are azimuthally symmetric, they are unable to directly tap expansion free energy stored in radial gradients and are thus excited exclusively via nonlinear process, such as "inverse cascade" of drift wave turbulence. Zonal flows are of great significance to confinement physics, since they are, effectively, sheared $E \times B$ flow layers which strain and distort the drift waves they co-exsist with [15].

Zonal flow shearing is the principle saturation mechanism operating in drift wave turbulence. Generic drift(or drift-ITG) turbulence may be modeled as a self-regulating, two component system, consisting of:

a) drift waves(with $k_\theta \neq 0$), which cause anomalous transport, and for which $\tilde{n}/n \sim e\tilde{\phi}/T$.

b) zonal flows with $k_\theta = 0$, for which $\tilde{n}/n \sim (k_\perp^2 \rho_s^2) e\tilde{\phi}/T$,which share available gradient free energy. The confinement regime quality is thus characterized by the branching ratio of zonal flow and drift wave energy.

2.2.1 Nonlinear Dynamics of Zonal Flows

The equation for the zonal flow intensity $U = |\phi_q|^2$ is modeled as

$$\frac{\partial}{\partial t} U + \gamma_d U = [Growth]U + [Noise].$$

Here γ_d reffers to the collisional damping, $[Growth]U$ refers to amplification due to drift-wave coupling and [Noise] refers to incoherent emission of drift wave energy into the zonal flow. Since the drift wave gas must maintain a divergence-free radial current (composed of polarization and transport-induced currents) and since the zonal shear flows modulate the transport-induced current, it follows that zonal flow stability is determined by:

$$\rho^2 \frac{\partial}{\partial t}(\partial_r^2 \phi) + \frac{\partial}{\partial r}\left[\frac{\delta \langle J_r \rangle}{\delta \phi} \phi\right] = 0 \qquad (15)$$

Here ϕ is the zonal flow potential, $\langle J_r \rangle$ is the transport-induced radial current and ρ is the polarization screening length. Since the radial current is simply the difference of electron and ion radial flux, it follows that the frequency Ω_q of a zonal flow mode with radial wavenumber q is

$$\Omega_q = -\left(q^2 \rho^2\right)^{-1} \left(q \delta \Gamma_- / \delta \phi_q\right) \qquad (16)$$

Here Γ_- is the relative flux. Γ_- is very detail-sensitive, since it involves the dissipative couplings of the various species. However, the generalized quasi-linear wave energy theorem (Poynting theorem) directly relates Γ_- to radial wave energy density flux at stationarity. Thus, the zonal flow frequency can be written as:

$$\Omega_q q^2 \rho^2 = -iq^2 \frac{\delta}{\delta \phi_q}\left[\rho_s c_s \sum_{\underline{k}} k_\theta \frac{\partial \epsilon}{\partial k_r}\Big|_{\omega_{\underline{k}}} \left|\frac{e\tilde{\phi}_{\underline{k}}}{T}\right|^2\right] \qquad (17)$$

Here $\underline{k}$ and $e\tilde{\phi}_{\underline{k}}/T$ refer to drift waves ($k_\theta \neq 0$) and ϵ is the difference of the real part of ion and electron susceptibilities. For simple drift wave models, $\partial \epsilon / \partial k_r \sim -k_r \rho_s^2$ so $\omega \sim k_\theta k_r |e\tilde{\phi}/T|^2 \sim \langle \tilde{v}_r \tilde{v}_\theta \rangle$, the Reynolds stress. Thus, zonal flows are seen to arise from modurations of the drift wave Reynolds stress.

The appropriate adiabatic invariant for drift wave turbulence in azimuthally symmetric shear flows is

$$N(\underline{k}) = (1 + k_\perp^2 \rho_s^2)^2 \left|\frac{e\tilde{\phi}_{\underline{k}}}{T}\right|^2 \qquad (18)$$

N is, in general, the (conserved) potential enstrophy Ω and is equal to the classical action only for the special case of (zonal flow)-(drift wave) interaction, for which k_θ is constant. Thus, the zonal flow growth rate may be written as

$$\Omega_q q^2 \rho^2 = -iq^2 \rho_s c_s \sum_{\underline{k}} k_\theta \frac{\partial \epsilon}{\partial k_r} \frac{1}{(1 + k_\perp^2 \rho_s^2)^2} \frac{\delta N}{\delta \phi_q} \qquad (19)$$

The quantity $\delta N / \delta \phi$ may be straightforwardly computed via linearization of the wave kinetic equation

$$\frac{\partial}{\partial t} N + (\underline{v}_g + \underline{V}) \cdot \underline{\nabla} N - \frac{\partial}{\partial \underline{x}} (\omega + \underline{k} \cdot \underline{V}) \cdot \frac{\partial N}{\partial \underline{k}} = \gamma(k) N - \Delta\omega(k) N^2 \qquad (20)$$

Here $\underline{v}_g$ is the drift wave group velocity, $\underline{V}$ is the zonal flow,$\gamma(k)$ is the drift wave growth rate and $\Delta\omega(k)N^2$ represents a damping of drift wave quanta due to local nonlinear coupling to damped scales. Linearizing eq.(20) finally yields the zonal flow growth rate

$$\gamma_q = -\frac{\rho^2}{\rho_s^2} q^2 c_s^2 \sum_{\underline{k}} \left[\frac{(k_\theta^2 \rho_s^2)(k_r \partial \langle N \rangle / \partial k_r)}{(1 + k_\perp^2 \rho_s^2)^2} \times R(\underline{k}, q)\left(1 - \frac{q^2 \rho^2}{1 + k_\perp^2 \rho_s^2}\right)\right] \qquad (21)$$

where $R(\underline{k}, q)$ is the resonance function

$$R(\underline{k}, q) = \gamma_{\underline{k}} / \left(\gamma_{\underline{k}}^2 + (\Omega_q - q V_g(k))^2\right) \qquad (22)$$

and V_g refers to the radial component of the wave group velocity.

The noise emitted into the zonal flow may be determined by calculating the incoherent mode coupling into modes with q_r finite and $q_\theta = q_z = 0$. For a simple plasma model(classical polarization), the calculation is

most efficiently done using two dimentional hydrodynamics. The result is:

$$\frac{\partial}{\partial t}|\phi_q|^2|_{noise} = (q^2c_s^2)\sum_{\underline{k}} \rho_s^4 \frac{(k_r^2k_\theta^2)^2}{(k_\perp^2)^2}\frac{\langle N\rangle^2 R(\underline{k},q)}{(1+k_\perp^2\rho_s^2)^2} \quad (23)$$

Note that the noise resembles the square of Reynolds stress, as it should. The zonal flow spectrum equation thus finally is:

$$\Big(\frac{\partial}{\partial t}+\gamma_d\Big)|\phi_q|^2 = \Big(-q^2c_s^2\sum_{\underline{k}}\frac{(k_\theta^2\rho_s^2)f(q\rho)}{(1+k_\perp^2\rho_s^2)^2}k_r\frac{\partial\langle N\rangle}{\partial k_r}R(\underline{k},q)\Big)|\phi_q|^2 + q^2c_s^2\sum_{\underline{k}}\rho_s^4\frac{(k_r^2k_\theta^2)^2}{(k_\perp^2)^2}\frac{\langle N(\underline{k})\rangle^2}{(1+k_\perp^2\rho_s^2)^2}R(\underline{k},q) \quad (24)$$

where $f(q\rho)=\rho^2/\rho_s^2[1-q^2\rho^2/(1+k_\perp^2\rho_s^2)]$.

Zonal flows shear and distort the drift wave spectrum which drives them. Thus, the zonal flows constitute a random strain field which randomly refracts drift waves, causing a diffusive increase in k_r which in turn enhances their coupling to small scale dissipation. The quasi-linear equation is given by

$$\frac{\partial\langle N\rangle}{\partial t}-\frac{\partial}{\partial k_r}D\frac{\partial\langle N\rangle}{\partial k_r}=\gamma(\underline{k})\langle N\rangle-\Delta\omega(\underline{k})\langle N\rangle^2 \quad (25)$$

where

$$D=\sum_q k_\theta^2q^2\left(1-\frac{q^2\rho^2}{1+k_\perp^2\rho_s^2}\right)^2(\rho_sc_sq)^2R(\underline{k},q)|\phi_q|^2. \quad (26)$$

¿From eqs.(24) and (25), we obtain zero-dimensional model for $U=|\phi|^2$ and $\langle n\rangle=\langle N\rangle/(\rho_s^2/L_\perp^2)$ as

$$\frac{\partial U}{\partial t}+\gamma_dU=\sigma\langle n\rangle U+[Noise] \quad (27)$$

$$\frac{\partial n}{\partial t}=\frac{c_s}{L_\perp}[\delta-\langle n\rangle]\langle n\rangle-\alpha\langle n\rangle U \quad (28)$$

where $\gamma_d\simeq\nu_{ii}/\sqrt{\epsilon}$, $\sigma\sim(q\rho_s)^2c_s/L_\perp\delta$ and $\alpha=(q^2c_s^2)(q^2\rho_s^2)/(\delta c_s)/L_\perp$. The stable fixed point in these equations is the finite flow state with

$$\left|\frac{\tilde{n}}{n}\right|^2\sim\delta\left(\frac{\rho_s}{L_\perp}\right)^2\frac{\gamma_d}{(c_s/L_\perp)}\frac{\overline{k_\theta^2}}{\overline{q^2}} \quad (29)$$

which corresponds to a thermal diffusivity

$$\chi\sim D_{GB}\left[\delta^2\frac{\gamma_d}{(c_s/L_\perp)}\frac{\overline{k_\theta^2}}{\overline{q^2}}\right] \quad (30)$$

where $D_{GB}=\rho_s^2c_s/L_\perp$, the gryo-Bohm diffusion coefficient. A striking feature of these results is the explicit proportionality of the fluctuation level and transport coefficient to the collisional flow damping $\gamma_d\sim\nu_{ii}$. This is a consequence of the fact that the flow is both driven by, and also regulates the strength of, the drift wave spectrum. Hence, increased collisional damping of the zonal flow makes it more difficult to excite the flow and to saturate the drift waves, thus leading to increased transport in this model.

3. Kinetic-Fluid Model for Drift Wave

To investigate the interaction between universal drift wave and convective cell in shearless slab geometry, kinetic-fluid model [11,12] is derived. To derive the model, we assume the distribution function is maxwellian in $v_\perp$ space and integrate the nonlinear gyro-kinetic equation [17] over the velocity space. The linear closure relation is used for the first moment of $v_{//}$ which ensures the exact linear dispersion relation. The ion continuity equation is written by

$$\frac{\partial}{\partial t}n_k-i\omega_*\Gamma_{0k}\zeta_iZ_i\phi_k+\tau(1+\Gamma_{0k}\zeta_iZ_i)\frac{\partial}{\partial t}\phi_k+\frac{\tau}{2}\times\sum_{k=k'+k''}(b\cdot k''\times k')\phi_{k'}\chi_{k''}(n_{k''}+\tau\phi_{k''})=0, \quad (31)$$

and the electron continuity equation is

$$\frac{\partial}{\partial t}n_k-i\omega_*\zeta_eZ_e\phi_k-(1+\zeta_eZ_e+k^2\lambda^2)\frac{\partial}{\partial t}\phi_k+\frac{\tau}{2}\times\sum_{k=k'+k''}(b\cdot k''\times k')\phi_{k'}(n_{k''}-k''^2\lambda^2\phi_{k''})=0, \quad (32)$$

where n_k is the fluctuating ion density and ϕ_k is the electrostatic potential, $\omega_*=\tau k_y\rho_i^2/(2L_n)$ is the normalized diamagnetic drift frequency by the ion cyclotron frequency Ω_i, ρ_i is the ion gyro-radius, $\tau=T_e/T_i$ is the ratio of electron and ion temperature, $\lambda^2=\tau\Omega_i^2/(2\omega_{pi}^2)$, ω_{pi} is the ion plasma frequency, $\Gamma_{0k}=I_0(b_k)e^{-b_k}$ with $b_k=k_y^2\rho_i^2/2$, $Z_{i,e}$ are plasma dispersion function with the argument $\zeta_{i,e}=\omega/(k_zv_{th\,i,e})$ and $\chi_{k''}=2\int_0^\infty dxxe^{-x^2}J_0(b_k^{1/2}x)J_0(b_{k'}^{1/2}x)J_0(b_{k''}^{1/2}x)/\Gamma_{0k''}$, where I_0 is 0-th order modified Bessel function and J_0 is 0-th order Bessel function. The factor 1/2 in eqs.(31) and (32) appears due to the definition of thermal velocity. The Poisson equation is used to eliminate the fluctuating electron density in the electron continuity equation [10].

The energy conservation relation is obtained from eqs.(31) and (32)as

$$\sum_k\Bigg(Re(s_2)\frac{\partial}{\partial t}|\phi_k|^2+2Re(s_1)|\phi_k|^2-2Im(s_2)\times Re(\phi_k)Im(\dot{\phi_k})-Im(\phi_k)Re(\dot{\phi_k})\Bigg)=0 \quad (33)$$

where Re shows real part, Im shows imagenary part of the argument, $s_1=i\omega_{*e}(\zeta_eZ_e-\Gamma_0\zeta_iZ_i)$, $s_2=1+\zeta_eZ_e+k^2\lambda^2+\frac{T_e}{T_i}(1+\Gamma_0\zeta_iZ_i)$ and $\dot{\phi}=\frac{\partial\phi}{\partial t}$. In the fluid ion and

near adiabatic electron response $1 \ll \zeta_i, \zeta_e \ll 1$, i.e., $v_{th\,i} \ll \frac{\omega}{k_z} \ll v_{th\,e}$, it is reduced to

$$\frac{\partial}{\partial t}\left(\sum_{k_x,k_y,k_z \neq 0} \{1 + k^2\lambda^2 + \tau(1-\Gamma_{0k})\} |\phi_k|^2 + \sum_{k_x,k_y,k_z=0} \{k^2\lambda^2 + \tau(1-\Gamma_{0k})\} |\phi_k|^2 \right) = 0. \quad (34)$$

The first term in LHS (left hand side) represents the drift wave energy and the second term represents the convective cell energy. In the same limit, the dispersion relation of universal drift wave is analytically evaluated as

$$\omega = \frac{\omega_* \Gamma_{0k}}{1+\tau(1-\Gamma_{0k})} + i\frac{(1+\tau)\omega_*\sqrt{\pi}}{(1+\tau(1-\Gamma_{0k}^2))^2} \times \left((1-\Gamma_{0k})\zeta_e e^{-\zeta_e^2} - \Gamma_{0k}\zeta_i e^{-\zeta_i^2} \right). \quad (35)$$

The dispersion relation shows that the universal drift wave is destabilized by the inverse Landau damping and is stabilized by the ion Landau damping. Based on this model, the universal drift wave turbulence is investigated numerically and is discussed in the next Chapter.

4. Simulation results

4.1 Numerical Scheme

Eqs.(31) and (32) are solved as follows. Initially the linear eigenvalue ω and eigenfunction are calculated for given parameters, then ω is fixed as a constant in plasma dispersion function. Now, eqs.(31) and (32) are formally expressed by the following equation

$$\frac{\partial}{\partial t} Y_k + f(Y_k, Y_k) + AY_k = 0 \quad (36)$$

where $Y_k = \{\phi_k, n_k\}$, A is a numerical constant including plasma dispersion function. The time step is advanced by the predictor-corrector scheme. Nonlinear Landau damping is not taken into account in this scheme, however, it might be possible if $A = A(\omega)$ is advanced in time numerically.

In present numerical simulations, the following parameters are used: $16 \times 32 \times 8$ modes in k_x, k_y, k_z space, $k_{x0} = k_{y0} = 0.15$, $k_{z0} = 0.02$, $m_i/m_e = 1836$, $\Omega_i^2/\omega_{pi}^2 = 10$, $\rho_i/L_n = 0.2$(the wave number is normalized by ion gyro-radius). Fig.6 shows k_y dependence of the real frequency, which is normalized by the ion cyclotron frequency Ω_i, and growth rate of universal drift wave in the cases with $k_x = 0.15$ and 2.4 for $k_z = 0.02$, respectively. It is shown that the universal drift wave is unstable in the short wavelength region (large-$|k_y|$). Larger $|k_x|$ makes the universal drift wave more stable. It should also be mentioned that for larger k_z, the universal drift wave is stable.

4.2 1D and 2D Spectra of Energy

To investigate the normal cascade and inverse cascade processes in the wave vector space, we define the following power spectra according to eq.(34). The energy spectrum in k_z space of drift wave is defined by

$$E_{DW}(k_z) = \sum_{k_x,k_y} \{1 + k^2\lambda^2 + \tau(1-\Gamma_{0k})\} |\phi_k|^2 . \quad (37)$$

Then the drift wave energy E_{DW} and the convective cell energy E_{CC} are written by

$$E_{DW} = \sum_{k_z} E_{DW}(k_z), \quad (38)$$

$$E_{CC} = \sum_{k_x,k_y,k_z=0} \{k^2\lambda^2 + \tau(1-\Gamma_{0k})\} |\phi_k|^2 . \quad (39)$$

In the components of Fourier modes which constitute the convective cell, the zonal flow component corresponds to $k_x \neq 0, k_y = k_z = 0$ and the streamer component corresponds to $k_x = k_z = 0, k_y \neq 0$. Similarly, 1-D(dimensional) and 2-D spectra of the potential and internal energy E_ϕ and E_n are defined by

$$E_\phi(k_z) = \sum_{k_x,k_y} |\phi_k|^2 , E_n(k_z) = \sum_{k_x,k_y} |n_k|^2 , \quad (40)$$

and

$$E_\phi(k_x,k_y) = \sum_{k_z} |\phi_k|^2 , E_n(k_x,k_y) = \sum_{k_z} |n_k|^2 , (41)$$

respectively.

4.3 Collisionless Simulation of Universal Drift wave

Fig.7 shows the time evolution of the drift wave energy E_{DW} and the convective cell energy E_{CC}. The energy of each mode with $k_z = 0.02, 0.04$, and 0.06 is also shown. The maximum growth rate of the drift energy comes from the longest wavelength mode with $k_z = \pm 0.02$. It is seen that the convective cell and the drift wave with short wavelength of k_z are also excited at $t \geq 800$. The amplitudes of these modes are seen to reach almost the same level as those with $k_z = \pm 0.02$ at $t \geq 1300$.

Fig.8 shows the time evolution of 1-D spectrum of the potential and internal energy as the function of k_z. Time slices of $t = 100, 200, ..., 1600$ are shown. It is seen that the convective cell grows after the excitation of $k_z \simeq \pm 0.06$ modes and the cascade occurs in k_z space, simultaneously. As is also seen from Figure 4.3, the spectrum are almost flat in k_z space at $t = 1300$. The normal cascade is observed in addition to the excitation of the convective cell.

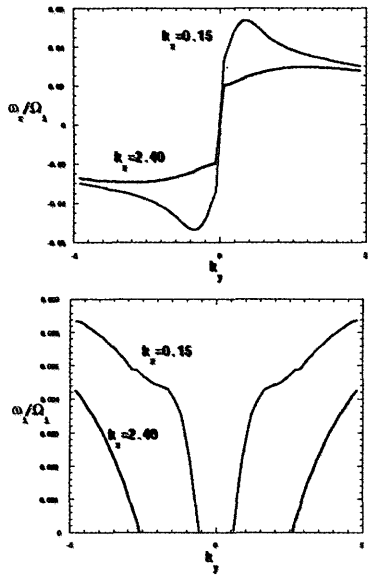

Fig. 6 k_y dependence of the real frequency and growth rate of the universal drift wave in the cases with $k_x = 0.15, 2.4$ for $k_z = 0.02$.

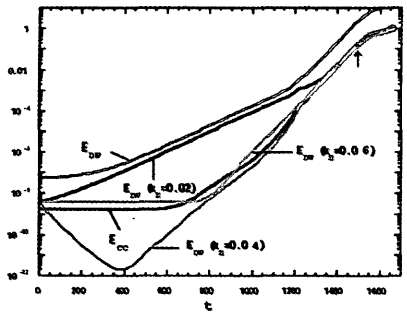

Fig. 7 Time evolution of the drift wave energy E_{DW} and the convective cell energy E_{CC}. The energy for each mode with $k_z = 0.02, 0.04, 0.06$ is also shown

Fig.9 shows the time evolution of 2-D spectrum of the potential and internal energy as the function of k_y for the case with $k_x = 0.15$. Time slices of $t = 10, 50, 100, 200, ..., 1600$ are shown. The cascade and inverse cascade occur in k_y space, the spectrum tends to be uniform at $t = 1400$. The excitation of zonal flow $k_y = 0$ is observed. This might be explained by the theory discussed in Chapter 2.

Fig.10 shows the 3-D power spectrum of convective cell energy of potential and density in k_y space at $t = 1500$. The corresponding time is marked in Figure 4.2 by the arrow. The excitation of zonal flow with $k_y = 0$ component in the potential energy is seen. The cases with $k_x = 0, \pm 0.15, \pm 0.30$ are plotted. It

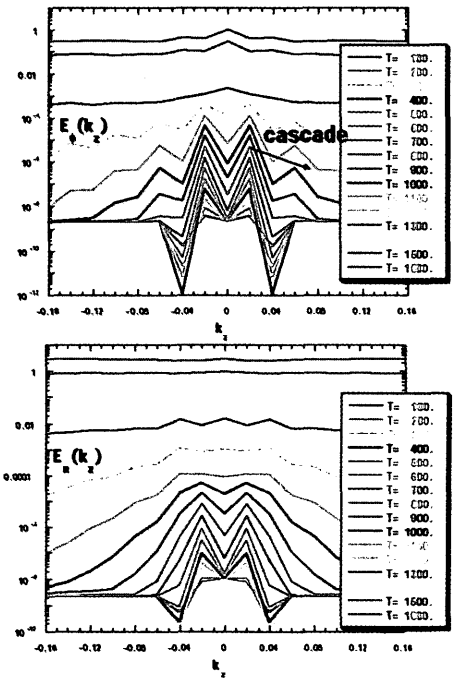

Fig. 8 Time evolution of 1-D spectrum of the potential and internal energy. Time slices of $t = 100, 200, ..., 1600$ are shown.

is clearly seen that the components of zonal flow with $k_x = \pm 0.15$ are dominant in the convective cell energy of potential. On the other hand, Fourier modes with $k_x = 0.3, k_y = 0.3$ and $k_x = -0.3, k_y = -0.3$ are dominant in the convective cell energy of density.

Fig.11 shows the time evolution of the Fourier modes in the convective cell energy of potential. The streamer with $k_y = 0.15$ is dominant in convective cell energy at $t = 1300$ as is indicated by the arrow. The zonal flow with $k_x = 0.15$ grows gradually and becomes dominant at $t \simeq 1600$.

Fig.12 shows the time evolution of the convective cell energy spectrum of density for finite k_x modes. This is plotted because the spectrum of E_n is different from the spectrum of E_ϕ. The modes with $k_x = 0.15$ and $k_x = 0.30$ are plotted for $k_y = 0.0, 0.15, 0.30$ and 0.45. It is seen that all Fourier modes in CC start to grow $t \simeq 600$. This is a clear identification of the nonlinear growth of CC with finite k_y modes.

Fig.13 shows the contour plot of the flux $\Gamma(x, y, z = 0)$ at $t = 390$ and $t = 1590$. The flux is calculated by the inverse Fourier transformation(which means the transforming a physical quantity from the wave vector space into the real vector space) of $\Gamma = \sum_{k=k'+k''} n_{k'}(-ik''_y \phi_{k''})$. Longitudinal or transverse axis is the y or the x axis, respectively. The red part

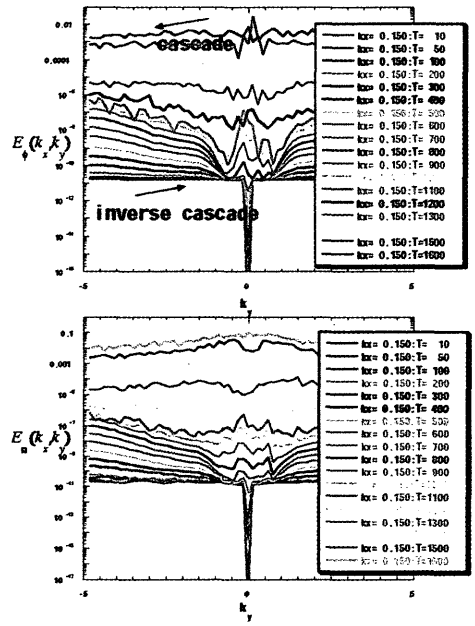

Fig. 9 Time evolution of 2-D spectrum of the potential and internal energy with $k_x = 0.15$. Time slices of $t = 10, 50, 100, 200, ..., 1600$ are shown.

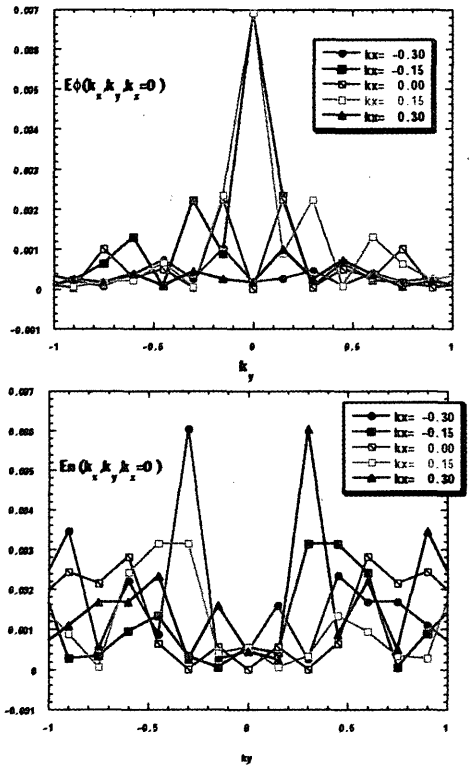

Fig. 10 3-D power spectrum of the convective cell energy of potential and density in k_y space at $t = 1500$. The cases with $k_x = 0, \pm 0.15, \pm 0.30$ are plotted.

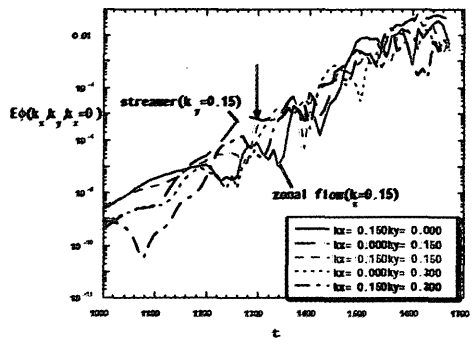

Fig. 11 Time evolution of Fourier modes in CC energy of potential

indicates high level of flux. It is seen that the large size vortex collapses into the small size elongated vortex at $t = 1590$. This collapse means that the irregular contour of flux(including the convective cell mode and the other modes) becomes eventually the similar level. These vortices move to the direction of $E \times B$, which are similar to the motion of the zonal flow.

4.4 Collisional Simulation of Universal Drift Wave

To investigate zonal flow damped by collision [5], the effect of ion-ion collision is investigated. It is included into the model equations by replacing $\frac{\partial}{\partial t} \to \frac{\partial}{\partial t} + \nu_{ii}$ in the ion continuity equation.

Fig.14 shows the time evolution of the drift wave energy E_{DW} and the convective cell energy E_{CC} in collisional case. It is found that the convective cell energy is more rapidly growing and is larger than the drift wave energy compared with those in collisionless case.

Fig.15 shows the 1-D spectrum of the potential energy E_ϕ and internal energy E_n as the function of k_z. Cascade occurs in k_z space and the convective cell is excited. It is found that the excitation of CC is stronger than that in collisionless case. The growth of linear drift wave is not clearly observed in spectral space.

Fig.16 shows the time evolution of 2-D spectrum of the potential and internal energy as the function of k_y for the case with $k_x = 0.15$. The cascade and inverse cascade occur in k_y space. It is found that the excitation of zonal flow is weak in this case. Other Fourier modes are dominant in CC energy as is shown in the next two figures.

Fig.17 shows the 3-D power spectrum of CC energy at $t = 800$ in the collisional case with $\nu_{ii} = 0.01$. The time $t = 800$ corresponds to the almost final phase of simulation and after that, the simulation breaks down due to the numerical instability. It is found that the zonal flow is damped by collision, however, the finite k_y

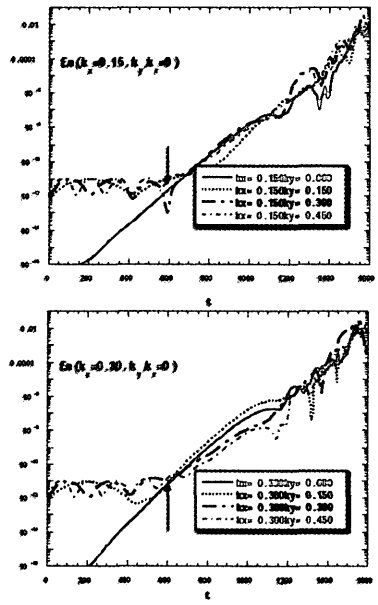

Fig. 12 Time evolution of Fourier modes in CC energy of density for finite k_y modes. The modes with $k_x = 0.15$ and $k_x = 0.30$ are plotted for $k_y = 0.0, 0.15, 0.30$ and 0.45.

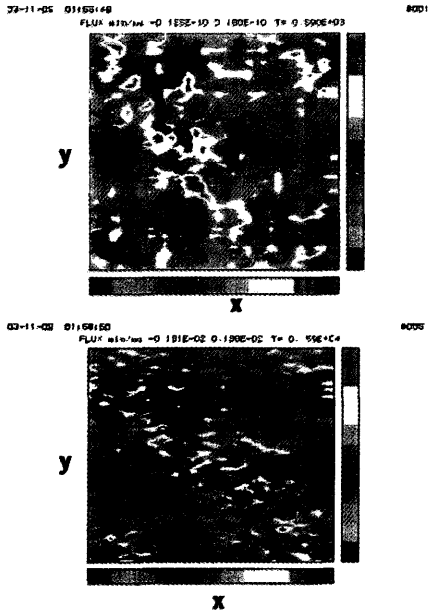

Fig. 13 Contour plot of the flux $\Gamma(x, y, z = 0)$ at $t = 390$ and $t = 1590$.

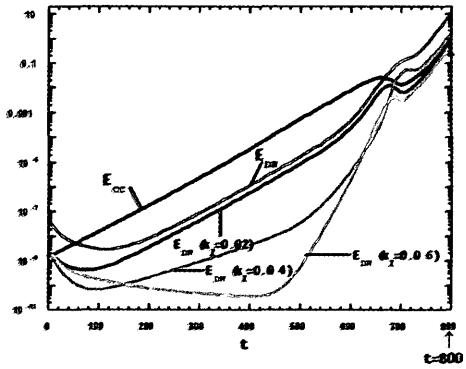

Fig. 14 Time evolution of the drift wave energi E_{DW} and CC energy E_{CC} for $\nu_{ii} = 0.01$(collisional-case). The energy for each mode with $k_z = 0.02, 0.04, 0.06$ is also shown.

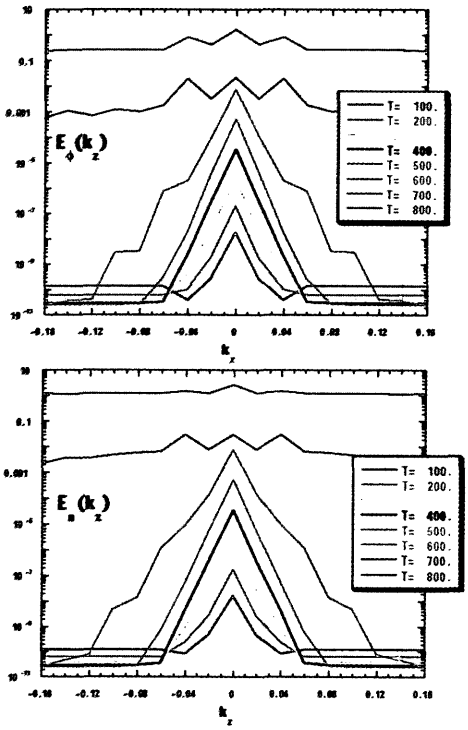

Fig. 15 Time evolution of 1-D spectrum of the potential and internal energy for $\nu_{ii} = 0.01$(collisional-case). Time slices of $t = 100, 200, ..., 800$ are shown.

modes are excited instead, which are large contribution of CC energy.

Fig.18 shows the time evolution of CC energy spectrum of potential for the case with $\nu_{ii} = 0.01$. It is seen that the component of streamer $k_x = 0.0, k_y = 0.3$ is dominant in CC energy in this case. Zonal flow $k_x = 0.15, k_y = 0.0$ gradually stays in quasi-steady state during $t = 670 \sim 720$, then starts to grow again. The collisional effect makes the zonal damping, however it also contributes to the excitation of other modes. The simple conclusion for saturation mechanism is not drawn in this case comparing to ITG case. The difference

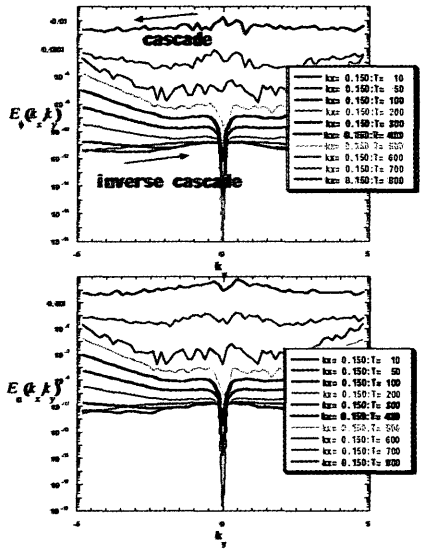

Fig. 16 Time evolution of 2-D spectrum of the potential and internal energy with $k_x = 0.15$ for $\nu_{ii} = 0.01$(collisional-case). Time slices of $t = 100, 200, ..., 800$ are shown.

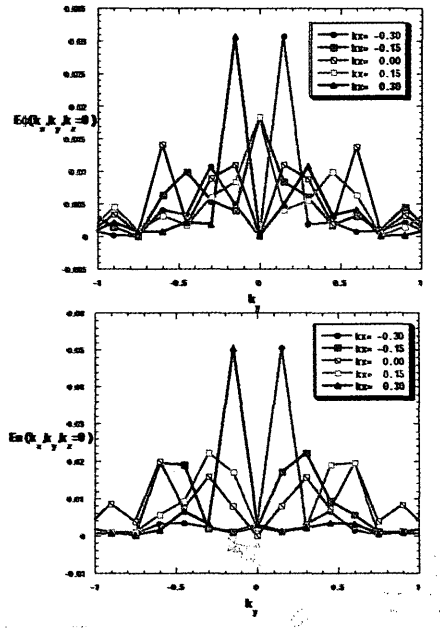

Fig. 17 3-D power spectrum of CC energy of potential and density in k_y space at $t = 800$ for $\nu_{ii} = 0.01$(collisional-case). The cases with $k_x = 0, \pm 0.15, \pm 0.30$ are plotted.

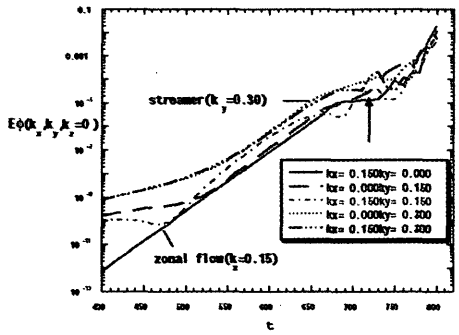

Fig. 18 Time evolution of Fourier modes in CC energy of potential for $\nu_{ii} = 0.01$(colisional-case).

might come from shearless and sheared slab geometry.

Fig.19 shows the time evolution of the CC energy spectrum of density for finite k_x modes in the presence of ion-ion collision ($\nu_{ii} = 0.01$). The modes with $k_x = 0.15$ and $k_x = 0.30$ are plotted for $k_y = 0.0, 0.15, 0.30$ and 0.45. For $k_x = 0.15$ modes, $k_y = 0.15$ mode starts to grow rapidly at $t = 500$ and reaches almost the same amplitude as other modes at $t \simeq 700$. For $k_x = 0.3$ modes, the growth of zonal flow and $k_y = 0.15$ mode is similar for $t \geq 500$ and both become dominant in $t \simeq 650$. The amplitude of the CC energy is almost the same as the one of collision-less case (Figure 4.7) when the CC energy starts to grow. Comparing the result in Figure 4.7 and Figure 4.14, we see that the time necessary to reach the same level is different. Namely, the collisional case is almost the half of the collisionless case.

Fig.20 shows the contour plot of the flux $\Gamma(x, y, z = 0)$ at $t = 490$ and $t = 690$ for $\nu_{ii} = 0.01$, respectively. The similar patterns are observed comparing with collisionless case. However, the vortex size is smaller than that in collisionless case.

Fig.21 shows the time evolution of convective cell energy and flux for the cases with $\nu_{ii} = 0$ and $\nu_{ii} = 0.01$. In the case with $\nu_{ii} = 0.01$, the growth of flux and convective cell energy is rapid compared to the one without collision, since the zonal flow is damped by collision. It is found that the flux and convective cell energy correlate to each other and reach almost the same levels. Streamer and finite k_y modes contribute to the flux in this collisional case.

5. Summary and Discussion

Kinetic-fluid model in the shearless slab geometry is introduced [10] using linear closure relation for the first moment of $v_{//}$, which is an extention of the model proposed by Smolyakov [8] and Hinton [9]. This model can simultaneously describe the universal drift wave turbulence and the convective cell dynamics, in which zonal flows and streamers are included.

Nonlinear simulations of universal drift wave turbu-

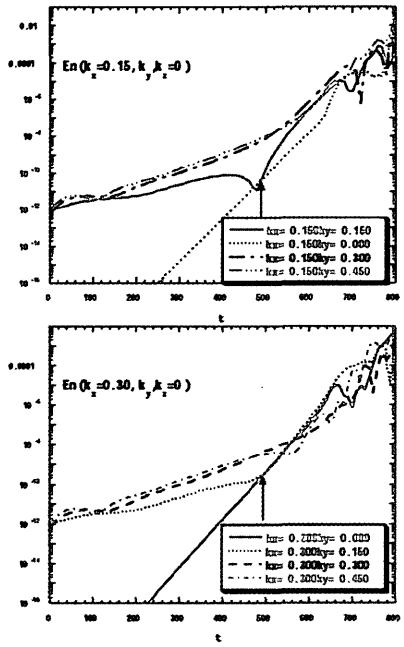

Fig. 19 Time evolution of Fourier modes in CC energy of density for finite k_y modes with ion-ion colision(ν_{ii} = 0.01). The modes with $k_x = 0.15$ and $k_x = 0.30$ are plotted for $k_y = 0.0, 0.15, 0.30, 0.45$.

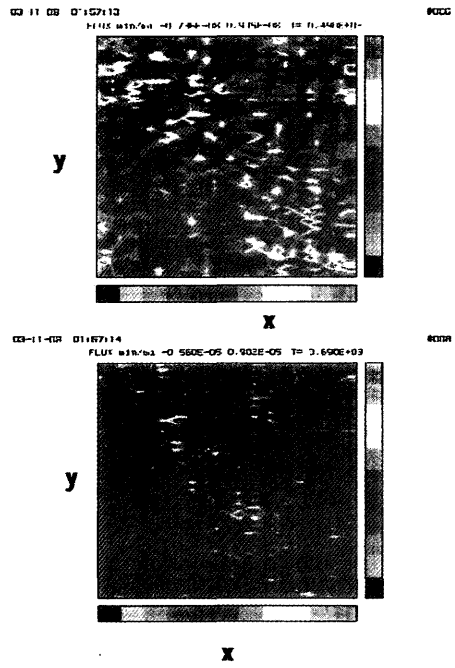

Fig. 20 Contour plot of the flux $\Gamma(x, y, z = 0)$ at $t = 490$ and $t = 690$ for $\nu_{ii} = 0.01$(collisional-case).

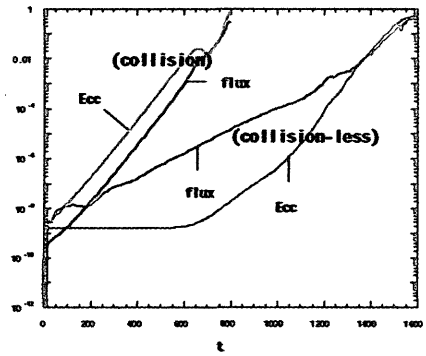

Fig. 21 Time evolution of CC energy and flux in cases with $\nu_{ii} = 0.0$ and $\nu_{ii} = 0.01$.

lence are performed for the collsional and collisionless cases by using this model. For the spectrum dynamics, the forward cascade is observed in k_z space and the forward/inverse cascade is observed in k_y space in the time evolution of energy spectrum. Simulation results show the excitation of convective cell. It is also observed that the ion-ion collision leads to strong excitation of CC energy and flux.

It is shown that the CC is nonlinearly excited which is similar to the case of zonal flow generation of ITG turbulence. However, no saturation is attained in our simulations. This is attributed from the fact that instability source exists in the short wavelength region of k_y space. On the other hand for ITG turbulence, the instability source exists in the long wavelength region and there is enough energy sink in the short wavelength region. Failure to attain the saturation in our simulation makes it difficult to compare results of the universal drift wave turbulence with the theory [2]. Furthermore, the theory assumes the marginally stable system to derive the model equations, then add the prescribed growth rate, arbitrarily. One possible way to avoid the numerical divergence is that we kill the instability and investigate the damped DW turbulence or initially we set finite amplitude of modes and investigate the nonlinearly self-sastained DW turbulence.

The ion-ion collision effect on zonal flow is also investigated. This effect makes the growth of CC energy stronger. It is concluded that the ion-ion collision damps the zonal flow and breaks down a self-regurating system between drift wave and zonal flow. It also excites the streamer and finite k_y modes, which dominate the amplitude of convective cell instead of the zonal flow. As the result, the flux is larger than the one without collision.

Fig.22 shows the flow diagram of the universsal drift

wave energy and convective cell energy. We have shown that the collision causes the damping of the zonal flow and the rapid excitation of streamer and other finite k_y modes. However, we don't know how much energy is transferred from of the universal drift wave to each Fourier mode (zonal flow, streamer and other finite k_y modes) in CC energy. It should be clarified. We should also explore the mechanism of the drift wave in sheared slab case and the zonal flow induced random shearing as possible nonlinear saturation mechanism [5, 16].

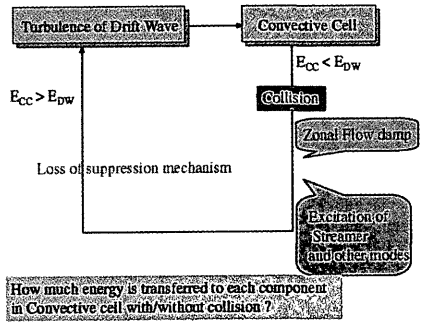

Fig. 22 Flow diagram about the universal drift wave energy and the convective cell energy.

References

1) A. M. Dimits, et al., Phys. Rev. Lett. 77, 71 (1996)

2) Z. Lin,T. S. Hahm, W. W. Lee, W. M. Tang, and R. B. White, Science 281, 1835 (1998)

3) A. Hasegawa, M. Wakatani: Phys. Rev. Lett. 59 (1987) 1581.

4) R. Z. Sagdeev, V. D. Shapiro and V.I. Shevchenko, Fiz. Plazmy 4, 55 1-559 (May-June 1978)

5) P. H. Diamond, M. N. Rosenbulth, F. L. Hinton et al., (1998) p.IAEA-CN-69/TH3/1.

6) L. Chen, Z. Lin and R. White: Phys. Plasmas 7 (2000) 3129.

7) C. Z. Cheng and J. R. Johnson: J. Geophys. Res. 104 (1999) 413.

8) A. I. Smolyakov, P. H. Diamond and M. Malkov: Phys. Rev. Lett. 84 (2000) 491.

9) F. L. Hinton, M. N. Rosenbulth,P. H. Diamond and L. Chen :APS, 41st Annual Meeting of DPP, Seattle 1999 UP166H.

10) private communications with M. Yagi and C. Z. Cheng (2002-2003)

11) C. Z. Cheng and H. Okuda, Phys. Rev. Lett. 38, 708 (1977)

12) A. A. Galeev, V. N. Oraevskii, and R. Z. Sagdeev, Zh. Eksp. Teor. Fiz. 44, 903 (1963) [Sov. Phys. JETP 17, 615 (1963)].

13) F. H. Busse, CHAOS 4, 123 (1949).

14) R. Z. Sagdeev, V. D. Shapiro and V.I. Shevchenko, Sov. J. Plasma Phys. 4, 306 (1979).

15) V. B. Lebedev, et. al., Phys Plasmas 2, 4420 (1995).

16) T. S. Hahm et al., Phys. Plasmas 6 (1999) 922.

17) E. A. Frieman and L. Chen, Phys. Fluids 25 502 (1982)